Hunting for Exoplanets with TESS and Observations

Daniel Teubenbacher

Submitted to the

Institute of Physics

Geophysics, Astrophysics and Meteorology (IGAM)

in Fulfilment of the Requirements of the Degree

Bachelor of Science

at the

University of Graz, Austria

Matriculation number: 01414953

Supervisor: Dr.Thorsten Ratzka

Graz, August 2018

Abstract

Ever since, humans wanted to know: Are we alone in the universe? Nowadays we possess the technologies that might answer this question. We speak here of extrasolar planets, short exoplanets. At the end of the 20th century the first ones were detected and by August 2018 more than 3800 exoplanets have been confirmed. With both, ground- and space-based missions, researches try to discover these foreign worlds. Firstly, this thesis gives an introduction into exoplanets and possible detection methods. The most successful method, measuring the temporary dip of the light curve of a transiting exoplanet, is of special interest because it paves the way for the Transiting Exoplanet Survey Satellite (TESS), the successor of the Kepler satellite. The current TESS mission is the main focus of this work and will be discussed in detail. There is also a practical part discussing the data of two exoplanet transits which were observed at the Observatorium Lustbühel in Graz.

Seit jeher wollten die Menschen wissen: Sind wir allein im Universum? Heute besitzen wir möglicherweise die Technologien, um diese Frage beantworten zu können. Die Rede ist von extrasolaren Planeten, kurz Exoplaneten. Die ersten wurden Ende des 20. Jahrhunderts entdeckt und bis heute konnte man bereits über 3800 bestätigen (Stand: August 2018). Mit Hilfe von Observatorien auf der Erde und Satelliten versucht man diese fremden Welten zu entdecken. Diese Arbeit beginnt mit einer kurzen Einführung zu Exoplaneten und den möglichen Detektionsmethoden. Die erfolgreichste Methode, bei der die temporäre Abnahme des Signals in einer Lichtkurve bei einem Planetentransit gemessen wird, ist von besonderer Relevanz, da diese die Grundlage für den Transiting Exoplanet Survey Satellite (TESS), den Nachfolger von Kepler, ist. Das Hauptaugenmerk der Arbeit liegt auf der aktuellen Mission von TESS, welche im Detail erläutert wird. Des Weiteren gibt es auch einen praktischen Teil, bei dem die Daten zweier Exoplanetentransits, die am Observatorium Lustbühel in Graz gemessen wurden, ausgewertet und diskutiert werden.

Content

1. Introduction – What is an Exoplanet?

A so-called extrasolar planet, short exoplanet, is a planet out of our solar system but in the gravitational field of another star. This means exoplanets are part of other planetary systems.

Stellar companions with low, planetary masses were long suspected, but as the detection requires very high accuracies, first planetary-mass objects were not discovered until the late 1980s. A first undisputed detection of an exoplanet was made in 1992 by Aleksander Wolszczan and Dale Frail using pulsar timing variations (see Chapter 2.4). Moreover, a breakthrough in spectroscopic observation methods allowed detections with the radial velocity (Doppler) method with very high accuracies. Nowadays this method is one of the two most successful ones. The first detection of a planetary-mass object around a main-sequence (sun-like) star was reported in 1995. (Perryman, 2011, p. 15)

Since then, various methods to detect exoplanets have been developed and have permanently been improved in accuracy. As of July 2018, more than 3800 exoplanets were discovered and confirmed.[1] With TESS and other upcoming missions, this number will rise very quickly in the near future.

Nowadays, exoplanet research is an emerging scientific field, not least because there are great opportunities allowing not only the proof of the existence of exoplanets, but also their characterization. Planets classes comprise the types we know from our own solar system (terrestrial planets, gas planets and gas giants) and also new discoveries like "Hot Jupiters" which are similar to our gas giants but orbit at a much smaller distance around their host star. Other types are "Hot Neptunes" (like Hot Jupiters but with lower mass) or "Super Earths" which are mostly terrestrial planets with masses higher than the Earth's mass but lower than the mass of Uranus. (Kaltenegger, 2015)

Discoveries of special interest are terrestrial planets in the habitable zone of their host stars. Water on these planets can exist in its three states. This is the first very important step to allow life based on the same chemical compounds as we know it. Some planets in the habitable zone have been found yet but extra-terrestrial life is still waiting to be discovered.

On the one hand, this thesis gives an introduction into exoplanetary science, detection methods, problems that arise etc., and on the other hand, it describes the TESS mission and its goals in detail. Observational data are also presented to illustrate the transit method used by TESS.

[1] from http://exoplanet.eu/catalog/

2. Exoplanet Detection Methods

There are several methods to detect exoplanets, 6 of which will be explained to get a glimpse on the procedures. One method is the Direct Imaging of exoplanets whereas the other ones are indirect methods, namely: Transit method, Radial Velocity (Doppler) method, Gravitational Microlensing, Astrometry and the (Pulsar) Timing method. The most successful methods are the Transit method, about 74% of all discovered exoplanets were found with this method, and the Radial Velocity method with about 20%. The ranking is followed by the other methods, each contributing $<2\%$.[2] As only the Transit method is relevant for this thesis, the explanations of other methods is kept short. For further information see, e.g., Perryman (2011).

2.1 Radial Velocity Method

If a planet orbits a star, a so-called "reflex motion" occurs. This means both planet and star orbit around the center of mass of the whole system resulting in a "wobble" of the star. Reflex motions can be determined by precise Doppler measurements as the wavelength and frequency, respectively, of the electromagnetic radiation of the star observed from earth shifts, when the star moves back and forth. By this data, shape and period of the planet's orbit, as well as information about the planet's mass is provided.

This method has been proven to be very successful in finding and also confirming exoplanets being detected with other methods in the first place.[3]

2.2 Astrometry

Similar to the Radial Velocity method, the possible reflex motion of a star is observed. Astrometry is generally requieres taking images and comparing the distances to reference stars. Nevertheless, the minuscule motion of the star is very difficult to detect and therefore Astrometry has not been very successful yet.[4]

2.3 Gravitational Microlensing

Using Einstein's interpretation of gravity, the concept of spacetime, this method can be visualized very well. As a heavy object, e.g., a star, warps spacetime, light passing near the star changes direction. In some cases, light can be focused and therefore magnified (see Figure 1). When a star (1) passes in front of another distant star (2) close to our line-of-sight, the distant star's (2) light can get focused and therefore

[2] from http://exoplanet.eu/catalog/

[3] from https://exoplanets.nasa.gov/5-ways-to-find-a-planet/#/1

[4] from https://exoplanets.nasa.gov/5-ways-to-find-a-planet/#/5

magnified. If a planet orbits star (2), its gravity can contribute to the magnification resulting in a local maximum in the magnification time diagram.

These microlensing events are not predictable, occur only once and can also happen due to so-called "rogue planets", which a planetary-mass objects directly orbiting a galactic center without a corresponding sun. (Wright & Gaudi, 2012)

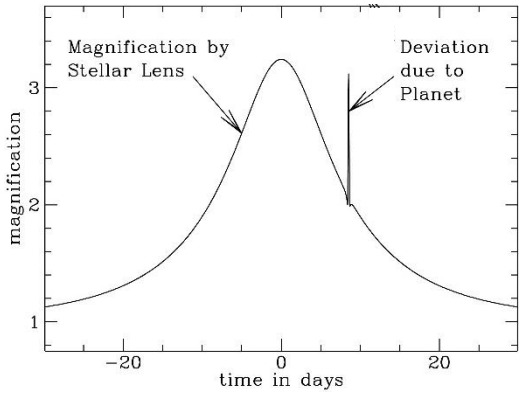

Figure 1: Diagram of a microlensing event with a planet orbiting the magnifying star (Gaudi & Bennett, 2011)

2.4 Timing Method

Pulsars, pulsating variables, eclipsing binary stars and even stars that host a transiting exoplanet show a periodic photometric variability. Timing variations can occur due to exoplanets. These variations can be caused by a Doppler shift, analogous to the Radial Velocity method, by light travel time variations and gravitational perturbations. The light travel time effect occurs when the orbit of a star around the center of mass is so large, that the time the light travels in addition becomes noticeable. If a planetary system has more than one planet, "transit timing variations" can be used to differentiate and/or confirm planets. (Wright & Gaudi, 2012)

The variation caused by different light travel times is most successfully used with pulsars as their pulse arrival times are very accurate.

2.5 Direct Imaging

The apparently easiest method to find exoplanets is to just take images of them. The problem is not that the planets are very faint (their brightness results from the reflection of the stellar emission and the thermal emission of the planet itself). Instead, the complication lies in the ratio of the planet's and star's brightness. The stars are usually millions of times brighter, outshining the planet. A method used to block the star's direct light is to use coronagraphs.[5]

[5] from https://exoplanets.nasa.gov/5-ways-to-find-a-planet/#/3

Less than 100 planets have been found yet via direct imaging.[6] Nevertheless it is a method which provides spectra of the planets and is therefore capable of characterizing a planet's atmosphere. Knowing the atmospheres is the only way to finally prove the habitability of terrestrial planets in the habitable zones.

2.6 Transit method

2.6.1 Overview

Last time, it happened on June 6th 2012 that Venus passed our line-of-sight to the sun. It was relatively easy to see the small black dot blocking some light of the sun for the duration of the transit. In our solar system we can see transits of Mercury and Venus occasionally as they are the inner planets from Earth's point of view. If we are lucky enough to have an exoplanet with its orbital plane lying extremely close to our line-of sight, it is possible to detect its transit. This transit produces periodic dips in stellar flux and reveals important system parameters like, e.g., orbital period, planet radius and furthermore also the mass of the planet. With additional Radial Velocity observations, the gravitational surface acceleration on the planet can also be determined.

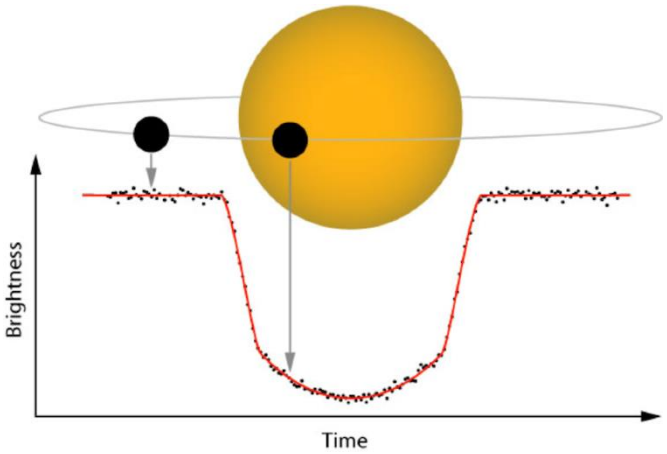

Figure 2: Schematic drop in stellar flux caused by a planetary transit *(Barclay, 2018)*

[6] from http://exoplanet.eu/catalog/

2.6.2 Transit Probabilities, Depths and Durations

An important parameter is the dimensionless impact parameter b. It describes the apparent distance of the planetary disc to the stellar disc at mid-eclipse. Assuming that the orbit is circular, the impact parameter reads:

$$b = \frac{a \cos i}{R_*}$$

where R_* is the radius of the stellar disc (see Figure 3). The impact parameter equals 0 when the transit happens to be central and 1 when the transit happens on the rim of the disc.

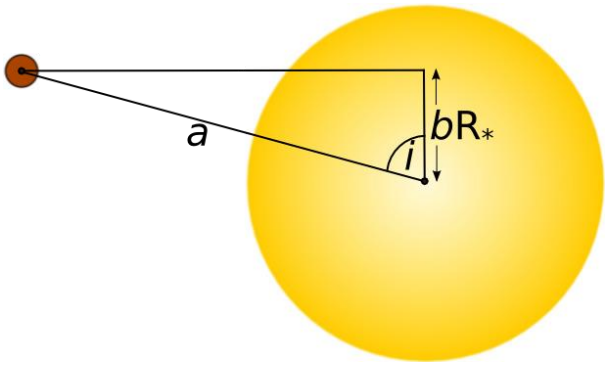

Figure 3: Impact parameter b in unit of the stellar radius R_*, i is the angle between the angular momentum vector of the orbit and the line-of-sight, a is the radius of the assumed circular orbit *(Wilson, 2017)*

In order for a full transit of a planet with radius R_p to occur $a^*cos\ i > R_* - R_p$ must be satisfied. A grazing transit happens when $R_* + R_p > a^*cos\ i > R_* - R_p$.

With this information, the (grazing or full) transit probability of a random oriented orbit can be expressed as:

$$\text{Prob}(\cos i < \frac{R_* + R_p}{a}) = \frac{1}{2}\int_{-(R_*+R_p)/a}^{(R_*+R_p)/a} = \frac{R_* + R_p}{a}$$

Typically $R_p \ll R_*$, therefore the transit probability simplifies to R_*/a or in unit of the solar radius $R_\odot$ and the astronomical unit au to:

$$Prob\ (\cos i < \frac{R_*}{a}) \cong 0.0046 \left(\frac{R_*}{R_\odot}\right)\left(\frac{1au}{a}\right)$$

The last equation means that the transit of earth is only visible from 0.46% of the celestial sphere. Hot planets near their host star are easier to discover, whereas for a planet with an orbit and size similar to Earth's, thousands of planets have to be observed over several years.

Transit depths, meaning the flux deficits at mid-transit, correlate to the ratio of the apparent areas of the planetary and the stellar disc.

$$\frac{\Delta f}{f} \cong \left(\frac{R_p}{R_*}\right)^2 = 0.0105 \left(\frac{R_p}{R_{Jup}}\right)^2 \left(\frac{R_*}{R_\odot}\right)^{-2}$$

As an example, the transit depth of Jupiter is about 1%. In practice limb darkening of the star's photosphere occurs and has to be considered too.

Figure 4 shows how a thermal-infrared light curve of a circularly orbiting planet looks like. The numbers 1 to 4 describe the different contacts while the span 1 to 4 is the total transit duration. During occultation, when the planet passes behind the star, it is the only time when the flux of the star alone can be determined. In between the transits and occultations, the planet's flux varies quasi-sinusoidally between the value where the hot dayside of the planet faces the observer and the value to which the cooler nightside contributes.

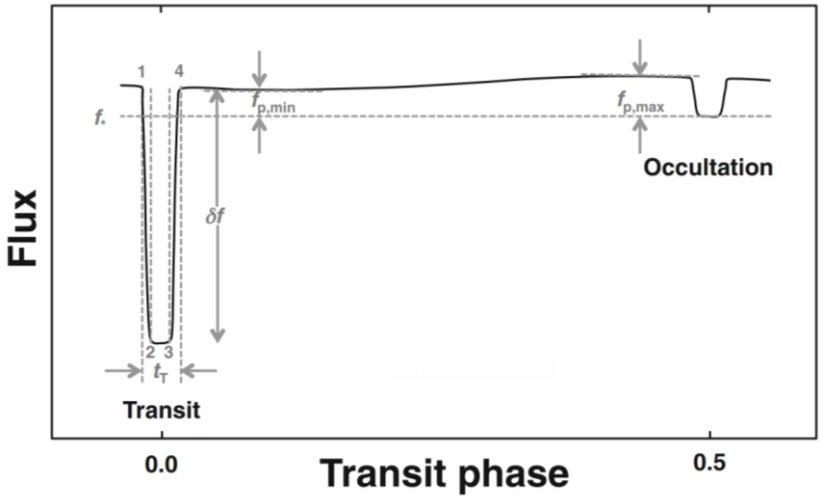

Figure 4: Thermal-infrared light curve of circular orbiting planet; 1,2,3,4: contact points; t_T = total transit time; f_* = flux level of the star (only at occultation when planet is behind star); $f_{p,min}$: nightside of planet faces observer; $f_{p,max}$ dayside faces observer (Cameron, 2016, p. 92)

Using Pythagoras' theorem, the length of the chord that the planet passes on the stellar disc during transit can be calculated. Knowing that the ratio of the transit duration to the orbital period is proportional to the ratio of the stellar radius to the orbital separation and applying Kepler's third law, the total transit duration for $\cos i \ll 1$ and a circular orbit becomes

$$\frac{t_T}{P} = \frac{R_*}{\pi a} \sqrt{\left(1 + \frac{R_p}{R_*}\right)^2 - b^2}$$

where P is the orbital period. For an exact derivation see Cameron (2016, p. 90ff).

2.6.3 Transit Surveys

With Radial Velocity surveys of F, G, K and M stars, the occurrence rate of gas-giant planets with orbits less than 0.1 AU is found to be about 1 %. These planets have high transit probabilities of order 2 - 10 % as they are close to their host stars and the transit durations are short enough (several hours) to be observed from ground within a night. Although these planets, hot Jupiters, are in fact rare, 1 in a 1000 stars should host such a transiting planet. To put it in perspective, discovering 1000 hot Jupiters requires the observation of 1 000 000 stars at minimum, assuming a detection efficiency of 100 %. The detection of smaller planets with larger separations to their host stars is even tougher as the transits might last longer than 10 h (Earth transit: 13 h) and the transit probability in general is considerably smaller than that of hot Jupiters for instance. (Cameron, 2016, p. 95)

Ground-based: A wide area of the sky has to be observed in order to discover exoplanets efficiently. Ground-based surveys therefore often use commercial camera tele lenses with a focal length of about 200 mm fixed on robotic mounts. The cameras used are science-grade charged coupled devices (CCDs). With these kind of surveys altogether about 80 % of the sky have been observed and over 180 gas-giant and ice-giant planets brighter than V = 13.0 with orbital periods of <10 days have been found and confirmed. The transatlantic exoplanet survey (TrES), the wide-angle search for planets (WASP), the Hungarian automated telescope network (HATNet) and the XO survey have been the most successful surveys of this kind. (Cameron, 2016, p. 95f)

Space-based: The detection of small planets with transit durations > 6 h is not possible via ground-based observation due to the lack of photometric precision, atmospheric transparency variations and even more importantly because of the length of the night. The transit depth of an Earth-sized planet is of the order 10^{-5}. Space-based missions allow a sub-pixel pointing accuracy and can be brought into an anti-solar orbit, either directly around the sun (Lagrange point 2) or in the orbit chosen for TESS for instance (see 5.4). (Cameron, 2016, p. 98)

2.6.4 False positives and candidate validation

A very important topic which has to be considered is False Positive (short FP) differentiation. False Positives are phenomena where a light signal suggests an exoplanet but in fact other astrophysical events cause the brightness dip. In contrast, false alarms are caused by transit-detection software failures. The software identifies a transit where there is none. The following chapter is based on Cameron (2016, pp. 116-119).

False positives make up about 50 % of the planet candidates which were discovered by Kepler. The percentage for TESS might even be higher due to its large Point Spread Function (PSF). Therefore the verification of TESS candidates as planets will be very important.

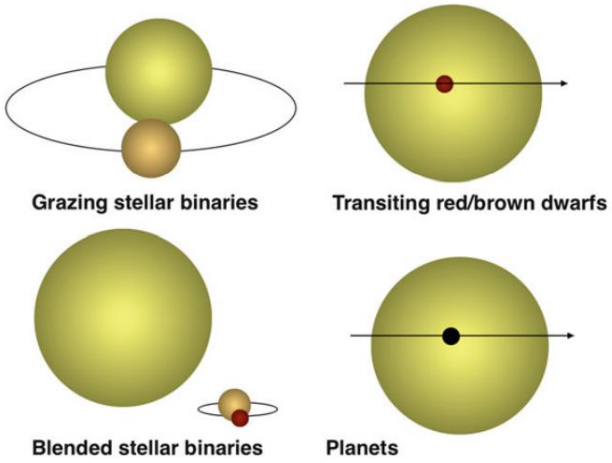

Figure 5: Different types causing transit-like events and a "real" planetary transit (right lower panel) (Cameron, 2016, p. 116)

Verification of actual planetary transits is based on statistics and is done by comparing the transit light curve with existing transit curves or by spectroscopic or multi-passband follow-up observations. Typical astrophysical FPs are shown in Figure 5 and described below.

Grazing binaries consist of two stars with similar masses and radii. A grazing transit of one star causes a significant V-shaped dip in the light curves. Also, the stars might have different effective temperatures and if follow-up photometry is available in multiple passbands, color-depended eclipse depths suggest that both objects of the binary system are self-luminous.

Transiting brown/red dwarfs can have very low masses and radii comparable to those of gas giants. This high inequality with their host star causes a flat bottom in the transit curve which might look like a planetary transit. Nevertheless, if the companion is self-luminous enough, secondary eclipses as well as the spectra of transiting objects might be detectable with high precision spectroscopy. Moreover, the dwarfs are massive enough to cause tidal elongation leading to synchronization of the host star's rotation. Optical variabilities due to a higher starspot activity arise. With precise light curves, e.g., from Kepler or TESS in the future, these variabilities as well as the tidal elongation can be figured out.

Blended stellar binaries might be coincidental alignments of a binary system and a star or a gravitationally bound triplet of stars. In the first type, a background binary system causes the light centroid to move towards the bright star during eclipse. This movement is characteristic to Kepler images. With ground-based astrometry these astrometric shifts can be detected. For a triplet system, this centroid shift is very small because of usually larger angular separations. (Bathala, et al., 2010)

In principle, the low spatial resolution of the comparatively small space-based telescopes require ground-based follow-up observations. These can again use multi-passband photometry to discriminate between eclipsing binaries and planetary transits.

Validation of exoplanet transits can be done by methods described above but also with other detection methods like radial-velocity follow-up for instance. However, e.g. the Kepler targets are too numerous to be effectively followed-up and validated separately. It is important thus to understand the statistical distributions of FPs. Several methods are being developed using statistical algorithms to evaluate whether a given candidate is more likely to be a planetary system or a FP. An alternative approach are coordinated observations distributed among many observatories.

3. Space-based survey examples

3.1 CoRoT

The first spaced-based mission to observe transiting exoplanets was CoRoT (short for Convection, Rotation and planetary Transits). The mission duration was 6 years, from 2006 to 2012. The orbit used for the spacecraft was a highly inclined 900 km polar orbit. CoRoT discovered 28 exoplanets with one of them, CoRoT-7b, being the first "super-Earth" because of its density and size similar to that of the Earth. (Cameron, 2016, p. 98f)

3.2 Kepler

The Kepler observatory was launched in 2009. Its main mission was set to last 3.5 years. It comprised a Schmidt-Type telescope with an aperture of 0.95 m. Kepler's photometer has a large FOV of 15 degrees in diameter covered with 42 CCDs. The main goals of the baseline mission were to find out the exoplanet distributions in planet size, planet orbits and the types of stars that host planets, as well as determining the percentage of terrestrial planets in or around the habitable zones of their host stars. In the course of the main mission, Kepler observed only one field in the sky (see Figure 6) (NASA, 2009)

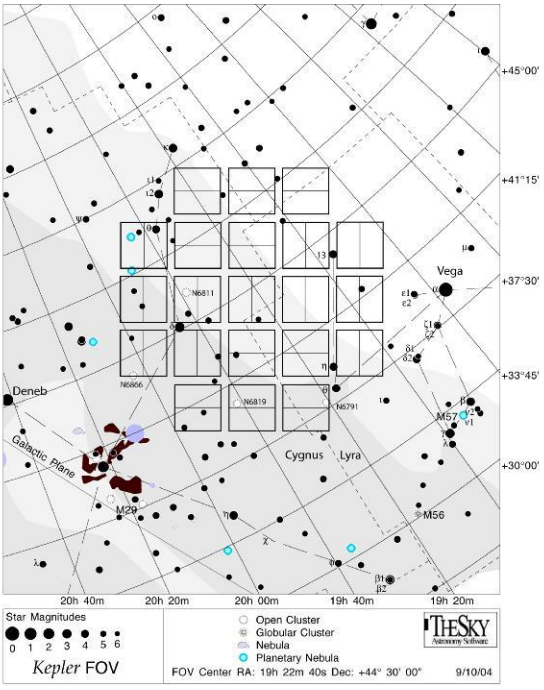

Figure 6: Field of View (FOV) of the Kepler baseline mission *(NASA, 2009)*

The Kepler main mission was able to detect over 4000 exoplanet candidates from which about 2000 are confirmed today. The primary mission ended due to the loss of two reaction wheels. Nevertheless a second mission, called K2, continued with observations near the ecliptic plane with different fields observed for about 3 months. Inaccuracies in pointing cause a lower photometric precision. Nevertheless, this precision can be restored by finer data reduction processes, albeit not as accurate as in the main mission. K2 discovered over 600 planet candidates of which about 200 have been confirmed to date. Comparing at the number of planet candidates and confirmed planets, one can notice how important follow-up investigation and False Positive determination is. (NASA, 2009) (Lissauer, 2018)

4. Ground-based observations at the Observatorium Lustbühel

To demonstrate a ground-based observation of an exoplanet transit and the regarding data reduction process, two examples will be discussed here. The observations were carried out at the Observatorium Lustbühel in Graz (+47° 03,9'N, -15° 29,7'E). The observatory is equipped with a 50cm f/9 Cassegrain guided telescope from Astro Systeme Austria. The attached STF-8300 CCD camera has a resolution of 3326 x 2504 pixels and is cooled to about -10°C to reduce thermal noise.

4.1 Preparation and Transit Event

With data from websites like the Exoplanet Transit Database[7], which provide exact transit times and depths for specific coordinates, follow-up observations of already known exoplanets can be realized. About one to two hours before the transit event begins, all instruments are turned on and calibrated and the telescope is pointed to the target star. Different kinds of images have to be taken in order to maximize the signal-to-noise ratio and thus the quality of the final product:

- *Raw-Frame:* Image, as it comes from the CCD.
- *Bias-Frame:* Image taken with zero exposure time and with the shutter closed. This is done to get the offset (artificial zeroing) of the pixel potential wells and to determine the read-out noise.
- *Dark-Frame:* Taken with the same exposure time as the Raw-Frame but with the shutter closed, this image allows the determination of thermal noise and dark current of the pixels. Nevertheless no darks where used for the following examples as the CCD was cooled (dark current negliable) and the exposure times were short and also varied in time.
- *Flat-Field:* By taking an image of an evenly illuminated are (in our case an image of the evening sky eastwards at about 45° height), variations of the pixel-to-pixel sensitivity across the CCD array as well as vignetting by the telescope or the filters can be removed. A flat-field frame must be produced for each filter.

Another important method to increase the sensitivity to maximize the signal-to-noise ratio and also to reduce the amount of data is called binning. During readout of the CCD, e.g., 4 pixels are combined to 1 (2x2 binning).

4.2 Data Reduction and Evaluation

After all images have been taken, the median of the bias-frames is subtracted from the raw-frames and the resulting images are divided by a normalized flat-field. Remaining "bad-pixels" are cleared with a routine that searches for pixels that are

[7] from http://var2.astro.cz/ETD

brighter than 5σ than their surrounding pixels (5x5 pixel box). If, for a pixel, this is the case, it is replaced by the mean of the enclosing pixels.

Moreover, to reduce the data, small frames, only containing the science target as well as the calibrator(s) are cut out separately. After that, aperture photometry is done. An annular aperture is put over the exact center of the target/calibrator. To get exact results, the background is determined by statistically averaging the pixels within an annulus and subtracting it from the summed count-rate.

4.3 HD189733

The observations of the star HD189733, located in the constellation of Vulpecula (the Fox), were made on August 18, 2015. A series of 5 V-band images with an exposure time of 2.5 sec alternating with 10 H-alpha images with 25 sec exposure time was obtained from 19:23:18.648 UT to 23:59:10.290 UT. For the data reduction only bias-frames were used, no darks and no flats.

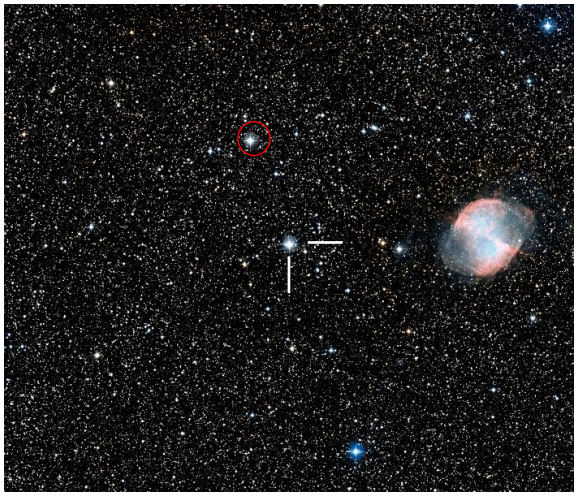

Figure 7: HD189733 (center) with calibrator HD 345459 (red) and the planetary nebula Messier 27 on the right. (ESA, 2007)

Figure 7 shows a field-of-view (FOV) of about 0.9° x 0.6° around the target. The normalized flux ratio of the science target HD189733 and the calibrator as well as their relative fluxes are separately shown in Figure 8. Ideally the flux ratio should always be constant until the transit happens, where the target gets dimmer and the flux ratio drops. For demonstration, the plots from Figure 8 only show the data from the H-alpha measurements, the plots are analogous for the V filter.

The dip and the zig-zag pattern in both the science and the calibrator data and the 'variable depth' of the transit are caused by problems with the dome of the observatory during the observation. The somewhat suspiciously decreasing flux ratio with respect to the beginning of the observations seems to be a general trend continuing after the transit. On the other hand, the elevation of the target was both increasing and decreasing during the observations.

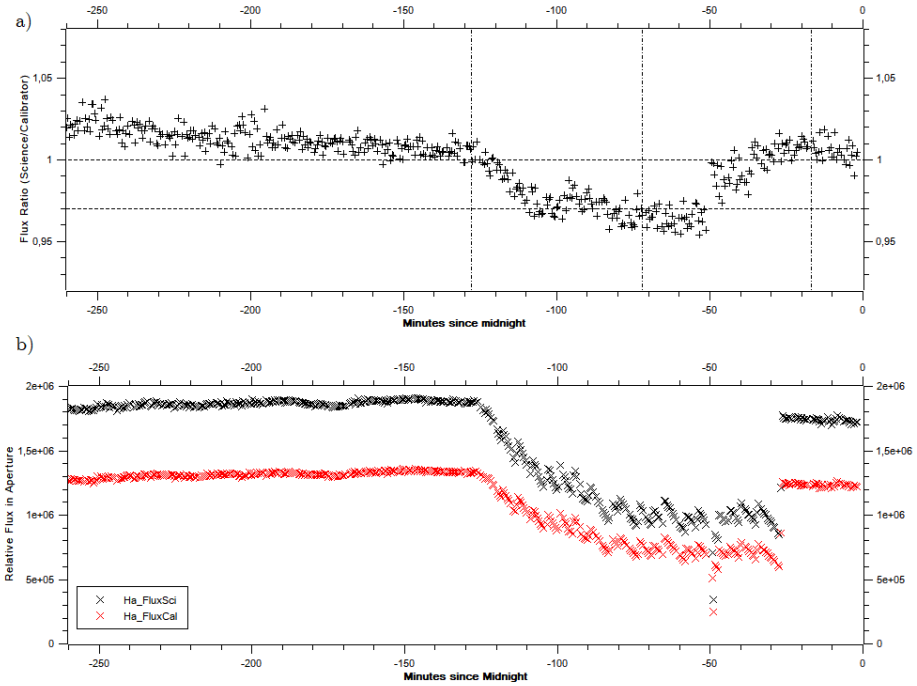

Figure 8: a) Flux ratio of science target HD189733 and calibrator with H-alpha filter (horizontal lines show the transit depth while the vertical lines indicate start, mid and end times of the transit); b) relative fluxes of target and calibrator (H-alpha)

The transit depth is about 3%, which is more than literature suggests: $(2.4122 \pm 0.0058)\%$.[8] With the relations shown in Chapter 2.6.2 and knowledge of parameters like stellar mass and radius, the radius of the planet and the inclination of the planetary trajectory can be calculated. The transit duration, 110 min, corresponds well to the literature value, (109.44 ± 2.45) min.[9]

4.4 WASP-85A

The science target on April 19, 2018 was the star WASP-85A located in the constellation of Virgo. Observations were done from about 19:50 UT to 01:00 UT.

Plots, similar to HD189733, are shown for the V-band in Figure 10 and the FOV around the science target with the used calibrator is shown in Figure 9.

[8] from http://exoplanets.org/detail/HD_189733_b

[9] from http://exoplanets.org/detail/HD_189733_b

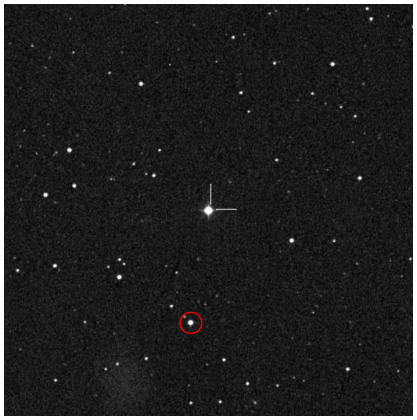

Figure 9: 0.25° x 0.25° image with WASP-85A in the center and the calibrator marked in red (MAST, 2008)

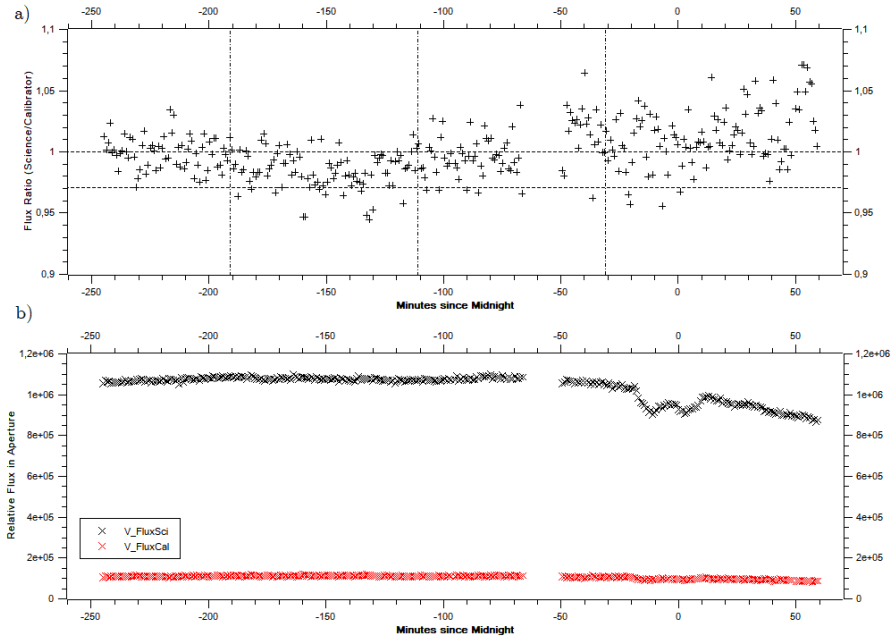

Figure 10: a) Flux ratio of science target WASP-85A and calibrator with V filter (horizontal lines show the transit depth while the vertical lines indicate start, mid and end times of the transit); b) relative fluxes of target and calibrator (V-band)

The calibrator of this observation was very faint (see Figure 10 b), therefore the transit is not clearly visible in the flux ratio plot. Nevertheless a transit depth of about 1-3% and a duration of 160 min can be estimated. The drop in flux of the science target at midnight is an artefact and the missing data at about 23:00 UT is due to data storage issues on the recording computer.

As one can see, transit observations from the ground can be quite difficult, mainly because of the higher noise level due to atmospheric perturbations and other error sources. This is one factor why it is reasonable to conduct space-based missions like CoRoT, Kepler or TESS for instance.

5. Transiting Exoplanet Survey Satellite (TESS)

5.1 Overview and Planning

The Transiting Exoplanet Survey Satellite, short TESS, is the successor of the Kepler observatory. The primary goal of TESS is to search for transiting planets (smaller than Neptune) around bright stars in the solar neighborhood. In fact, TESS searches for planets around the stars one can see when looking into the night sky with the unaided eye. In comparison to Kepler, TESS will perform an all-sky survey (90 % of the sky) with a search radius of about 200 light years, while Kepler observed only 0.25% of the sky but with a depth of as much as 3000 light years. As TESS targets are nearer and brighter, they will be perfect for follow-up science on earth and with future space telescopes (e.g. James Webb Space Telescope). (Barclay, 2018, 2014)

In late 2005, the first ideas for TESS came from the Massachusetts Institute of Technology (MIT) and the Smithsonian Astrophysical Observatory (SAO). There were some proposals to NASA about this mission but they were either neglected or did not manage to get enough funding. It took five years of proposals, planning and enhancing the plans until, in late 2013, TESS was selected as Explorer Mission with a cost cap of $200m. One of the reasons for the selection was the "cheap" highly inclined earth orbit. (Ricker, et al., 2014) In comparison, Kepler had a larger cost cap, the project life-cycle cost was approximately $600 million. Despite the orbit, there are also other cost-limiting factors like keeping the main mission duration at about two years and re-using software from the Kepler mission for instance. (NASA, 2009)

5.2 Spacecraft and Payload

TESS is made up of a spacecraft connected to the payload, which consists of 4 identical charge-coupled device (CCD) cameras with the same lenses and hoods. There is also a Data Handling Unit (DHU) which is the "brain" of the satellite. The spacecraft supplies power via two solar arrays and also provides a sunshield (see Figure 11). Regarding size, TESS is 1.5 m high, 1.2 m wide and 3.9 m long (sun arrays deployed; un-deployed: 1.2 m in length) and weighs 362 kg. All its parts, shown in Figure 1, will be discussed in detail below. (Spaceflight 101, 2018)

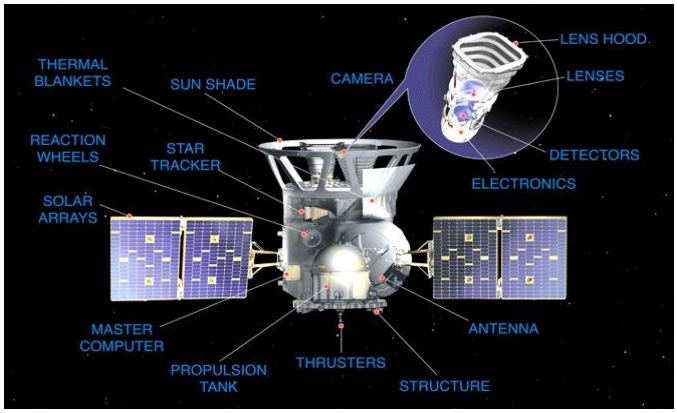

Figure 11: TESS assembly (Barclay, 2018)

The following description of the Transiting Exoplanet Survey Satellite was presented by the writer in the scope of the Emerging Researchers in Exoplanet Science Symposium (ERES IV) at Penn State University, USA, in June 2018. The corresponding poster is available at *homepage.uni-graz.at/de/thorsten.ratzka*.

5.2.1 Cameras and Lens Assembly

The four identical cameras have a field-of-view (FOV) of 24° x 24°. As they are shifted relatively to each other by 24°, a combined FOV of 24° x 96° (3200 deg^2) is accessible.

Beginning from the front, every camera has got a lens hood to prevent scattered light from earth and moon (there will not be scattered light directly from the sun see 5.4). The hood is followed by two aluminum barrels containing 4 and 3 lenses, respectively (see Figure 12). These lenses all have antireflection coatings and there are also stray light baffles between the lenses. One of these optical elements also has a long-pass filter coating which is necessary to produce a cut-off at 600 nm in the bandpass of TESS (see Chapter 5.2.2). Every lens assembly has an entrance pupil with a diameter of 10.5 cm. The focal ratio is f/1.4. (Ricker, et al., 2014)

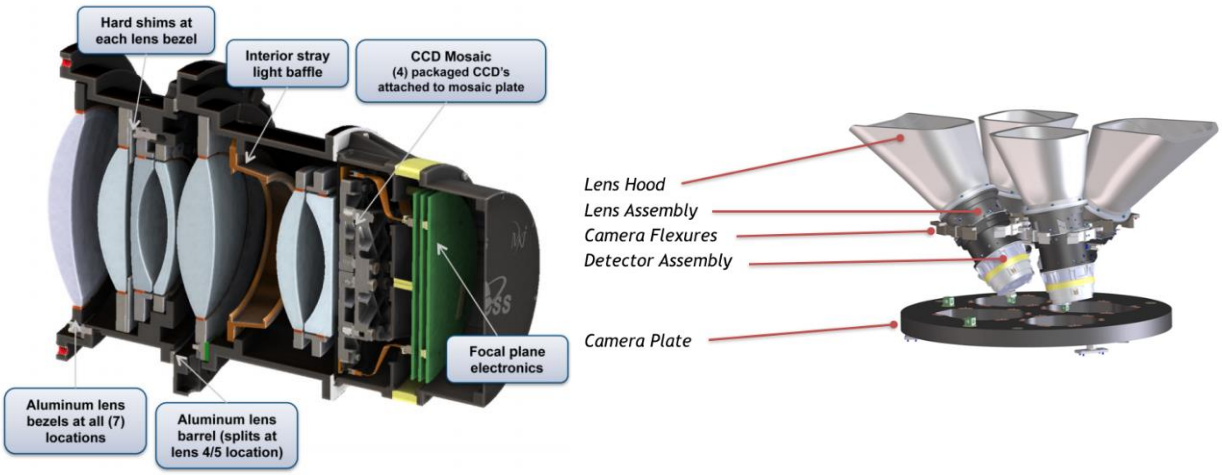

Figure 12: LEFT: TESS camera (without lenshood at the front) (Ricker, et al., 2014); RIGHT Mounting of the 4 cameras on a common plate (Barclay, 2018)

This special design of the lenses provide an un-vignetted image on the focal plane with consistent image spot size across the FOV. Like the Kepler observatory, the TESS cameras produce undersampled images. This results in a higher sensitivity as stars are kept on one or just a few pixels.[10]

The nominal operation temperature will be kept constant at about -75°C. At this temperature, the dark current is negligible. The expected 50% ensquared-energy half-width at the nominal focus is 15 microns. The ensquared energy describes the fraction of the total energy of the PSF (point spread function) that is within a square of a

[10] from http://www.sbig.de/universitaet/glossar-htm/sampling.htm

given length centered on the peak. So, pointed on the peak of the PSF, 50% of the energy is within a square of 15 x 15 microns, which represents 1 detector pixel. 90% of the energy will be within a square of 4 x 4 detector pixels (60 x 60 microns). A TESS pixel covers with 21" a wider area on the sky in comparison to the Kepler observatory (4" per pixel).

At the back of the lenses the detector assembly is located. Every camera has an array of 4 back-illuminated MIT/Lincoln Laboratory CCID-80 devices at the focal plane. TESS uses frame-transfer CCDs where only one half of the sensor is actually used for light collecting and the other (masked) half for saving the image (see Figure 13). This allows a fast shutterless readout of about 4 ms. Consequently, these sensors are twice as large compared to a full frame CCD with the same imaging array.[11] As mentioned above, the pixel size is 15 x 15 microns and one of the 4 imaging arrays has 2048 x 2048 pixels. With a separation of 2mm between the CCDs, one detector has 4096 x 4096 pixels and therefore a size of about 62 mm x 62 mm. Located beneath the focal plane, there are two circuit boards which will transmit the digitized data to the DHU. All four cameras are mounted on a common plate so that they are always aligned to form the 24° x 96° FOV.

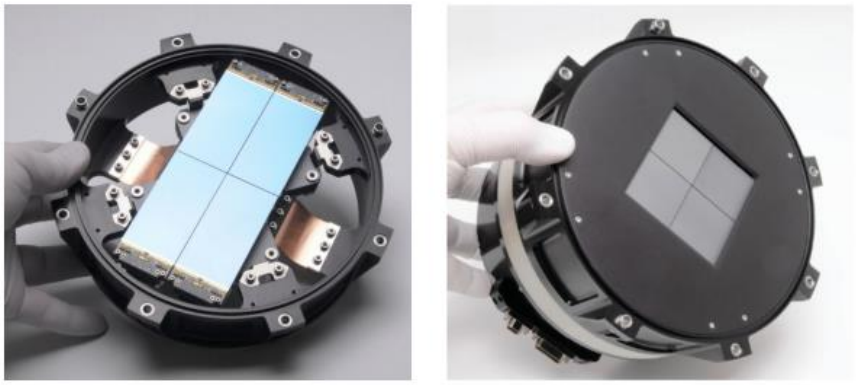

Figure 13: LEFT: Imaging array of 4 CCDs, RIGHT: Store regions of the CCDs masked (Schlieder, 2017)

[11] from http://www.andor.com/learning-academy/ccd-sensor-architectures-architectures-commonly-used-for-high-performance-cameras

5.2.2 *Bandpass*

The TESS detector bandpass ranges from 600 nm to 1000 nm. As already mentioned, a long-pass filter coating within the lens assembly produces the cut-off at 600 nm. The other limit is set by the quantum efficiency of the CCDs. This means the CCDs become less and less sensitive to incident photons of wavelengths longwards of 900 nm. The spectral response function is visualized in Figure 14. (Schlieder, 2017)

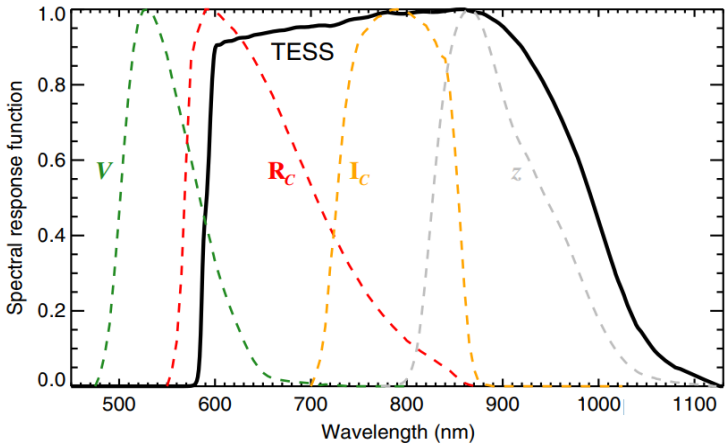

Figure 14: TESS detector spectral response function in comparison to other bandpasses (Ricker, et al., 2014)

This bandpass was specifically chosen to reduce photon counting noise. A wider bandpass has lower noise. Moreover, it is sensitive to the light of cool, red stars. The bandpass is centered on the conventional Cousins I-band (I_C) and also includes the R_C-band and the Sloan Digital Sky Survey z filter. (Ricker, et al., 2014)

5.2.3 Data Handling Unit

The Data Handling Unit, short DHU, is responsible for compressing and storing data from the cameras. It is also necessary for spacecraft avionics and ground communications. The CCDs of the cameras constantly produce 2 second exposures during science operation. Out of this data, the DHU compresses two kinds of images in real time. Firstly, 900 images are summed as 30-minute Full-Frame Images (FFIs) and stored on a 192 GB solid state recorder (SSR). Secondly, the images are summed in groups of 60 as 2-minute exposures, out of which, so called "Postage Stamps" are extracted and saved.

These Postage Stamps are subarrays of nominally 10 x 10 pixels and they are centered on preselected target stars (Ricker, et al., 2014). Per orbit, >10 000 Postage Stamps and >600 FFIs are created by each camera. Around 200 guide stars are tracked by the DHU for every 2 second exposure to calculate offset parameters for fine attitude pointing. (Schlieder, 2017)

5.2.4 Spacecraft

Under the payload section, the LEOStar-2 spacecraft bus from Orbital ATK is attached. It has a hexagonal shape on which numerous internal and external elements are fixed. On the outside are, e.g. the two solar arrays and a Ka-Band antenna dish. Thermal control is mainly achieved with thermal paint and blankets on the exterior. Excess heat is removed with heat pipes. In case of an unexpected cold period there are even survival heaters for the core electronics. The solar arrays are built to produce up to 415 W while the estimated total power needed is only about 290 W. At every perigee for a duration of 4 hours, the data from the SSR is downlinked with the Ka-band antenna dish with a data rate of up to 125 Mbs^{-1} (highest in the NASA Deep Space Network). Such a high data rate is only achievable because of the orbit with its close perigee. In comparison, the highest data downlinking speed of Kepler is about 0.53 Mbs^{-1} (NASA, 2009). If communication beyond the perigee position is needed, omni-directional S-band antennas are attached to the exterior. (Spaceflight 101, 2018)

In the inside of the hexagonal structure, the spacecraft has four reaction wheels (one is redundant) which are three-axis controlled for primary attitude control. Via the offset parameters from the DHU (see previous chapter), precise attitude corrections can be performed. The pointing accuracy is better than 3.2 arcsec and the stability is as good as 0.05 arcsec per hour. Due to problems with the Reaction Wheel Assembly of the Kepler mission, TESS' reaction wheels are built very robustly and withstand over 100 million hours operating in space.

Nevertheless, these offset parameters rely on the input from the cameras so the stabilization procedure described above only works in science mode. In non-science phases, the primary attitude determination sensor is a Micro-Advanced Stellar Compass "µASC Star Tracker Unit" which has two optical heads and one data processing unit. It captures the sky and analyses on board of TESS its exact three-axes orientation in space by comparing its images with precise star catalogues. An initial acquisition from a lost-in-space scenario takes 30 milliseconds and there are 8 measurements per second nominally. Measurements will be as accurate as 2 arcsec. Additionally, TESS has an inertial measurement system including four gyroscopes and sun sensors on the sun shade to obtain the sun vector. (Spaceflight 101, 2018)

Especially for orbit but also for attitude control, TESS uses a hydrazine monopropellant propulsion system comprising five thrusters and a hydrazine propellant tank. The tank is pressurized and thrust is produced by the decomposition of hydrazine as it passes a catalyst bed and creates gaseous products expelled at high pressure through a nozzle. The thrusters are located outside the bottom side of the spacecraft and the tank is inside the spacecraft. 45 kg of fuel are carried by the tank giving a delta-v budget of 268 m/s. Including initial orbit acquisition, TESS will need about 80% of the fuel for the two-year mission. In this budget also included are non-launch vehicle position corrections (e.g., solar wind pressure). (Spaceflight 101, 2018)

5.3 Launch and Orbit Design

TESS was launched on April 18, 2018 at Cape Canaveral Air Force Station in Florida aboard a SpaceX Falcon 9 rocket.[12] This is the first time a NASA science mission was launched with a SpaceX rocket. Falcon 9 is a 2 stage rocket with the speciality, that the first stage consisting of 9 Merlin 1D engines, is reusable as it is able to land back on (or near) the launch pad or on a floating platform. The second stage has one Merlin 1D engine. The Falcon 9 rocket has a payload of max. 22800 kg for Low Earth Orbits. TESS is a comparatively light and small payload. (Spaceflight 101, 2018)

TESS has a complex trajectory to get to its final science orbit, this is mainly because of cost reasons. As mentioned in the chapter above, TESS' delta-v budget is limited to 268 m/s. One constraint is to stay within this budget. Another constraint is to keep the perigee of the science orbit low enough for high speed data downlinking. On the other hand, high collision probabilities should be avoided and the apogee arc should allow long, undisturbed observation times. Moreover, eclipse durations should stay within a maximum of a few hours, because the number of batteries is also limited. (Dichmann, et al., 2016) Another consideration is an adequate thermal and radiation environment outside the Van Allen belts to maximize the detection sensitivity. (Spaceflight 101, 2018)

A solution which fulfils all these constraints is a highly eccentric orbit which is inclined by 28.5°. TESS will be the first satellite in this orbit with an apogee separation near 59 $R_\oplus$ and a perigee separation near 17 $R_\oplus$. (Dichmann, et al., 2016) The high inclination avoids long eclipse periods and the large separations keep TESS out of earth´s radiation belts. Finally, the science orbit will have a period of 13.7 days and will be in a 2:1 resonance with the moon. (Schlieder, 2017) This resonance means that each apogee is nearly 90° out-of-phase with the moon. Two wanted results are that the moon will not be in the FOV of TESS and also that the moon's gravitation acts on opposite directions, changing every half sidereal month and thus cancels itself out. Therefore the orbit is quite stable over years, only small corrections in the downlinking periods by the thrusters due to solar wind pressure are necessary. (Spaceflight 101, 2018)

To get to the final science orbit, several maneuvers have to be performed. TESS' trajectory timeline is shown in Figure 15 and a top-down diagram of the trajectory events can be found in Figure 16. For the following description it is recommended to have a look at these figures.

[12] from https://blogs.nasa.gov/tess/

After launch TESS will perform 3.5 phasing orbits which will last about 26 days. Followed by a Translunar Injection maneuver, TESS will perform a lunar flyby providing two important results. The new orbit is a Transfer Orbit with the apogee radius desired for the final orbit. Also the wanted inclination is achieved with this maneuver. This Transfer Orbit will have a PLEA (Post-Lunar-Encounter-Apogee) of 81 $R_{\oplus}$. Succeeding this event is the PLEP (Post-Lunar-Encounter-Perigee), the Time of Flight between these events is abbreviated with TOF. At the following perigee, a Period Adjust Maneuver (PAM) is performed to reach the lunar resonance of 2:1 and thus, operational orbital stability. Theoretically, it would be ideal to have the Moon-Earth-Vehicle angle 0° at PLEP, but calculations showed a maximum of 30° is acceptable at PLEP. The mission design allows correctional burns if there are errors during the planned maneuvers (see green dots in Figure 15). Until TESS reaches its science orbit (also called p/2 HEO orbit), 62 days pass by. (Dichmann, et al., 2016)

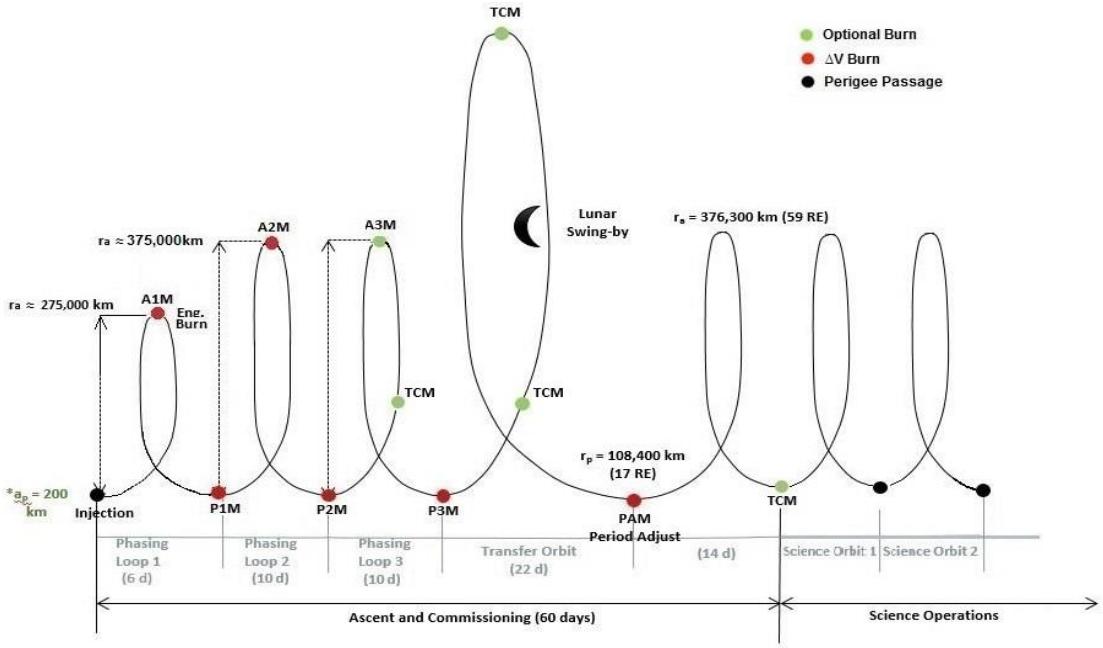

Figure 15: TESS trajectory timeline (Spaceflight 101, 2018)

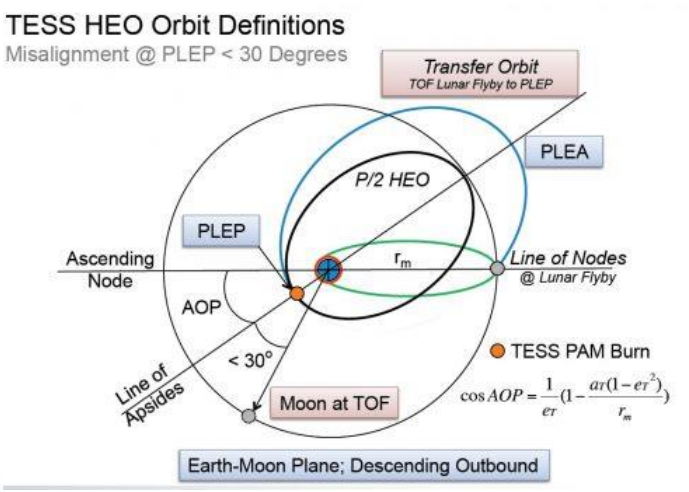

Figure 16: Trajectory events: PLEA (Post-Lunar-Encounter-Apogee), PLEP (Post-Lunar-Encounter-Perigee), TOF (Time of Flight), PAM (Period Adjust Maneuver), AOP (Argument of Periapsis), Final scientific orbit: P/2 HEO (Dichmann, et al., 2016)

It can be shown that for such an eccentric and inclined orbit, the Kozai-Mechanism applies. This means that eccentricity and inclination oscillate. Moreover, the orbital period will oscillate around the resonant orbit period because of the Sun's perturbations on the moon's orbit and thus on TESS' orbit. For further information on how the Kozai-Mechanism works, see Dichmann et al. (2016). Nevertheless, TESS' mission orbit is quite stable as these oscillations happen over periods of 8-12 years. (Schlieder, 2017)

5.4 FOV and Observing Strategy

As already mentioned in Chapter 5.2.1, the combined FOV of TESS covers a field of 24° x 96° on the sky. The main mission of TESS lasts two years, in which the northern and southern hemisphere will be observed each for one year. Starting in the south, TESS will work with the "stop and stare" method, meaning it will "stare" at one sector for the duration of 2 orbits (27.4 days), then rotate about 27.7° eastward, stare again etc. After 13 such observing sectors, TESS will rotate and inspect the northern hemisphere (see Figure 17 left side). Each sector begins at 6° off the ecliptic so that the uppermost detector array is centered on the ecliptic pole. This strategy with 26 sectors all together allows to cover over 90% of the sky. (Schlieder, 2017)

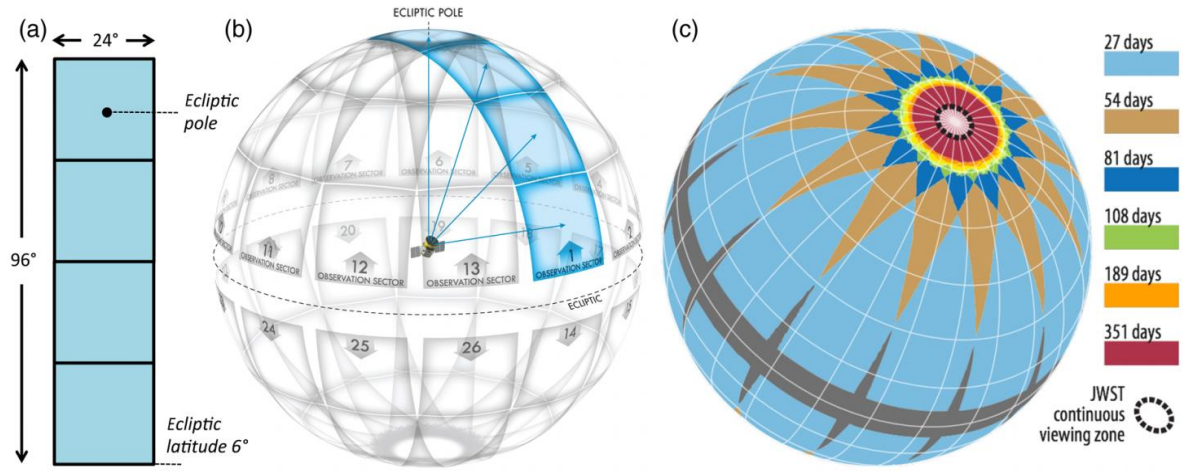

Figure 17: LEFT: Field of View (FOV) of TESS with observing sectors of the 2 year mission; RIGHT: overlapping sectors with the time coverage indicated (Ricker, et al., 2014)

By virtue of the constant width of the FOV, overlapping regions with longer observation times are formed (see Figure 17 right side). These overlaps even create a Continuous Viewing Zone (CVZ) at the ecliptic poles of about 900 deg^2 (Ricker, et al., 2014). The CVZ of TESS coincides with the CVZ of the James Webb Space Telescope, which will allow detailed investigations in the future. (Schlieder, 2017)

After commissioning, the first sector is chosen to be anti-solar, this way, by always rotating in an eastward direction, TESS' FOV will stay anti-solar throughout its entire mission (see Figure 18).

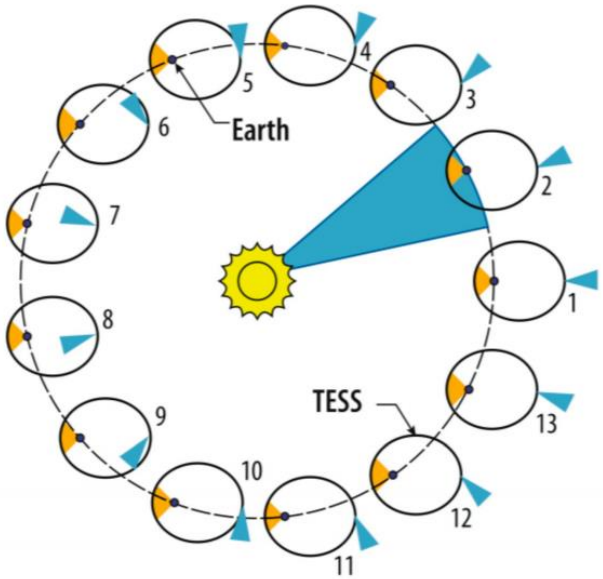

Figure 18: Schematic diagram of TESS' orbit, observing orientation (blue; always anti-solar) and downlinking periods (orange) for 1 year (Schlieder, 2017)

5.5 Which stars will be observed?

As mentioned above, there have been several successful surveys in the last years looking for extrasolar planets with different methods. With transiting planets, it is possible to find out details of these planets such as compositions and atmospheric properties. Ground-based transit surveys like, e.g., WASP or TrES concentrated on finding giant planets orbiting bright host stars. Due to the perturbations by the earth´s atmosphere, ground-based surveys always lack of photometric precision and therefore are not able to detect planets smaller than Neptune. Space missions, on the other hand, are not affected by these perturbations. The CoRoT and the Kepler mission had a high photometric precision and could therefore detect smaller planets. Nevertheless, as they concentrated on specific, small areas of the sky with longer observation times, these space surveys mostly detected transiting exoplanets of faint stars that are far away. The problem is that these faint exoplanets are not optimal for further investigation, i.e., finding out atmospheric properties. (Sullivan, et al., 2017)

The goal of TESS is to find exoplanets which can then be further explored via follow-up space-, and ground-based observatories. Therefore, TESS concentrates on (host) stars of spectral types F5 to M5 because these allow finding small planets around them. Hotter stars than F5 are not favourable, because they are large and small planets cause only a weak signal. Colder stars than M5 are also not optimal because they would be best observed at infrared wavelengths outside the TESS bandpass (see 5.2.2). (Ricker, et al., 2014)

5.5.1 Target selection

Before a specific target selection, it was necessary to gather all the stars TESS can detect, resulting in an all-sky catalog, the so-called TESS Input Catalog, short TIC. Including both, point and extended sources, every luminous and persistent object in the sky is included. Fast moving objects, like solar system objects are not included. Out of the TIC, a subset of target stars can be extracted and a specific calculation of the flux contamination of each star is possible. Additionally, the TIC provides data like the radii of the target stars which will be used for calculating planet radii. If required, researchers can look up stellar parameters like effective temperature T_{eff}, surface gravity (log g), mass (M*) and radius (R*) to calculate the properties of the detected planets. (Stassun, et al., 2018)

The TIC can also be used for false positive identification, which is going to be very important because there will be a high percentage of false positives. This catalog, with about half a billion objects, also serves as basis for the Candidate Target List (CTL), which is a subset of about 200 000 stars for the selection of the targets that will be observed with a 2 min cadence. These are chosen by simple stellar criteria. The CTL provides more detailed information for every potential target star. Deriving this

information is non-trivial and would be way too time consuming when applied to the whole TIC. All catalogs are available for the public at MAST[13]. (Stassun, et al., 2018)

5.5.2 TESS Input Catalog (TIC)

Several photometric catalogs where used to create the TIC. The description here is based on Stassun et al. (2018). Currently, as of June 2018, the full TIC-6 contains about ~ 473 million objects. It includes point sources (~ 470*10^6), such as stars, as well as extended sources (~ 2*10^6) like, e.g., galaxies. The remaining ~ 10^6 objects are from specially curated lists (described below). There a three base catalogs, which are merged to create the TIC:

For the point sources, the 2MASS point source catalog is cross matched with other, smaller, catalogs like, for instance, the catalogs also used for the Kepler mission. From different catalogs, information like the stars' proper motions, parallaxes and fluxes are extracted and combined for single matches. Sometimes there is, e.g., a 2MASS star for which two stars in the Gaia DR1 catalog exist. In such cases the coordinates are averaged and the mean of the fluxes of the Gaia stars are stored.

Extended Sources are included by a cross-match of the 2MASS extended source catalog, the ALLWISE and the SDSS extended source catalog.

Special Curated Lists: Objects from the Hipparcos catalog, lists for Cool Dwars, Hot Subdwarfs or bright stars as well as guest investigator targets and known planet hosts are added to the TIC regardless of cross matches with the other base catalogs.

Despite the target stars' position, the apparent magnitude in the TESS bandpass, hence abbreviated with T, is the most important and basic variable. Using the magnitudes from the existing catalogs and empirical relations, T can be calculated. These polynomial relationships with its error vary with the spectral type, gravity and metallicity of the different types of stars. An example for a polynomial relationship to calculate T can be found in the Appendix. As dwarfs are very important for the TESS mission, there are separate relations for surface gravities of log g $>$ 3, metallicities of [Fe/H] $>$ -0.5 and effective temperatures of Teff $>$ 2800 K. In astrophysics, the surface gravity is often expressed as log g by taking the base-10 logarithm of the surface gravity in cm/s^2, e.g., for earth: log g = 2.992. The metallicity is defined as the logarithm of the ratio of a star's iron abundance minus that of the Sun. This means negative values refer to a metallicity lower than the Sun's metallicity.

[13] from https://archive.stsci.edu/tess/

Reddening also plays a role in TESS observations. To describe this effect, the V magnitude (centered on 550 nm) of the stars is necessary. If it is not available right away from the catalogues, or there is a discrepancy between two catalogues, it is possible to calculate V from relations provided by comparing V magnitudes with the $G - K_S$ color in most cases. G and K_S mean the light through different passbands of a photometric system and G-K_S thus provides color information.

De-reddening is generally done by shifting colors along a so-called reddening vector e. g. in a J – H (again a color) to RPM_J (see Chapter 5.5.3) diagram to match empirical relations. It is only applied for dwarfs as they are especially important for the mission.

Another important variable one has to consider for the TIC is the effective temperature T_{eff} of a star. There are different correlations for giants and non-giants. An example of the determination of T_{eff} is given in the Appendix. For most stars, catalogs do not provide T_{eff}, i.e. this variable is derived by empirical relations of the $V - K_S$ color.

For the specially curated cool dwarf list in the CTL, the T_{eff} values are determined independently. A comparison of the T_{eff} values derived from the $V - K_S$ color and those from the Cool Dwarf List can be found in Figure 19.

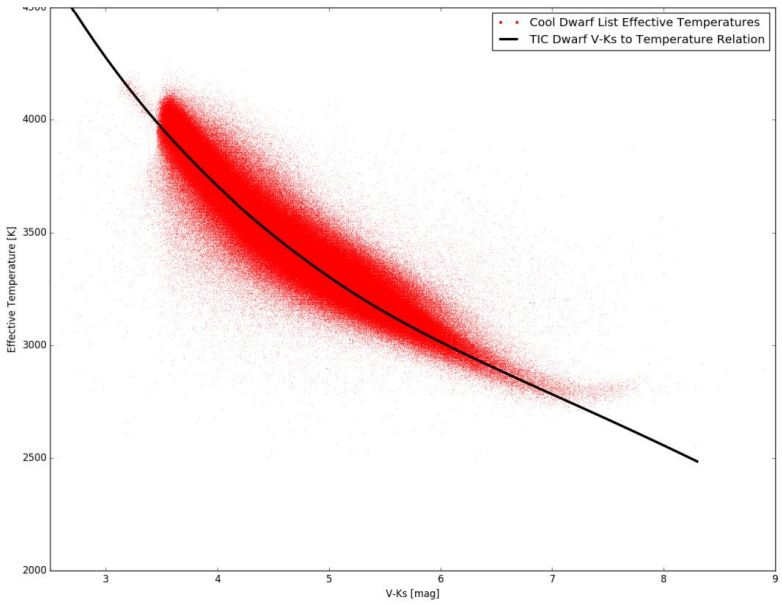

Figure 19: T_{eff} comparison between Cool Dwarf List and from TIC (Stassun, et al., 2018)

5.5.3 Candidate Target List (CTL)

The following description is again based on Stassun et al. (2018). It is necessary for TESS to preselect targets from the TIC for its 2-min cadence observations simply because the TIC contains too many objects that are not necessarily interesting for investigation. The primary demands of the mission are to search up to 200 000 stars for planets with orbital periods of less than 10 days and about 10000 stars in the ecliptic pole regions with orbital periods up to 120 days. These planets shall have radii less than 2.5 $R_{\oplus}$. It should also be possible to determine the masses for at least 50 planets with radii smaller than 4 $R_{\oplus}$. These demands are used to create a subset of the TIC, called Candidate Target List, short CTL.

Basically different cuts are applied on all the stars from the TIC like including dwarfs with the desired apparent magnitude and spectral type and excluding giants and evolved stars. After selecting, a prioritization scheme is applied to get the best choices for the 2-min cadence postage stamps.

Firstly, every star from the special curated lists is included in the CTL. If a point source of the TIC is not included in such a list it is part of the CTL if (T $<$ 12 and Teff $\neq$ 0) or (T $<$ 13 and Teff $<$ 5500 K). Furthermore, the stars should have a low probability to be giants according to the reduced proper motion (RPM) criterion. This criterion effectively separates dwarfs from giants but lacks in precision from differentiating dwarfs from subgiants. The contamination of apparent dwarfs by actual subgiants is 53%. The used J-band RPM is defined as

$$RMP_J = J + 5\log(\mu)$$

Where J is the magnitude in the J-band and μ is the total proper motion in arcsec per year.

Important is that giants have a much lower RPMs than dwarfs of the same color. (Gould & Morgan, 2003) A test of the RPM method for about 160,000 stars from the TIC with proper motions from Gaia DR1 can be found in Figure 20. Objects lying under the cut are included in the CTL.

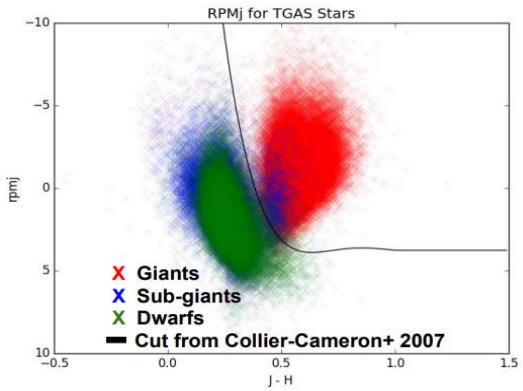

Figure 20: RPMj digramm with a cut defined by Cameron et al. (2007)

Stellar Radii and masses are necessary for the target prioritization, if they are no available from the special curated catalogs, they have to be calculated.

If the parallax of a star is known, one can estimate the stellar radius with the Stefan Boltzmann equation. Empirical relations are applied to get Teff and the bolometric luminosity. Incorporating the parallax, the stellar radius can be calculated and also log g can be derived.

Mass and radius of stars without parallax and with or without spectroscopic T_{eff} and log g are determined via empirical relations.

Last but not least, one of the main objectives of the CTL is to prioritize targets to maximize the discovery of small transiting exoplanets for the 2-min exposures of TESS. To define the quality of a transit signal the following signal-to-noise-ratio is used:

$$\frac{S}{N} = \frac{\delta}{\sigma}\sqrt{N_{data}}$$

δ is the fractional transit depth, σ is the photometric noise per data point and N_{data} is the number of data points during transit, which has a geometrical correlation to the total number of data points.

The photometric noise per data point depends on the stellar flux in the TESS bandpass where also light contamination, detector noise and background noise make a contribution. How much these errors add up also depends on where the star is located in the focal plane, because of TESS' point spread function (PSF) that actually varies over the detector array. Assuming the noise per data point is dependent on T (thus σ_T), the prioritization metric can be defined as:

$$\frac{\sqrt{N_S}}{\sigma_T R^{\frac{3}{2}}}$$

which is proportional to the signal-to-noise ratio mentioned above. N_S denotes the number of observing sectors the star is located in and R is the stellar radius. One can see that the priority rises for greater N_S (higher ecliptic latitude), because of the longer lasting observation periods in these regions. Objects within the Galactic plane ($|b| < 15$) are de-prioritized by a factor of 0.1 (see Figure 22), because there is a confusion between sources, creating significant errors in determining physical properties of the targets. This de-prioritization does not account for objects from the cool dwarf list because their physical parameters are known with low uncertainties. Stars located within 6° of the ecliptic do not have a priority as they are not part of any observing sector (see Figure 21).

If there is a fore-, or background star near the target star, an unwanted flux contamination is produced. Figure 22 shows a plot of the estimated contamination ratio for the objects in the CTL. A visualization tool[14] was used to create these plots. This ratio was evaluated with a contaminant search radius of 10 pixels (pixel size: 20.25") and TESS' PSF is assumed to be a 2D Gaussian.

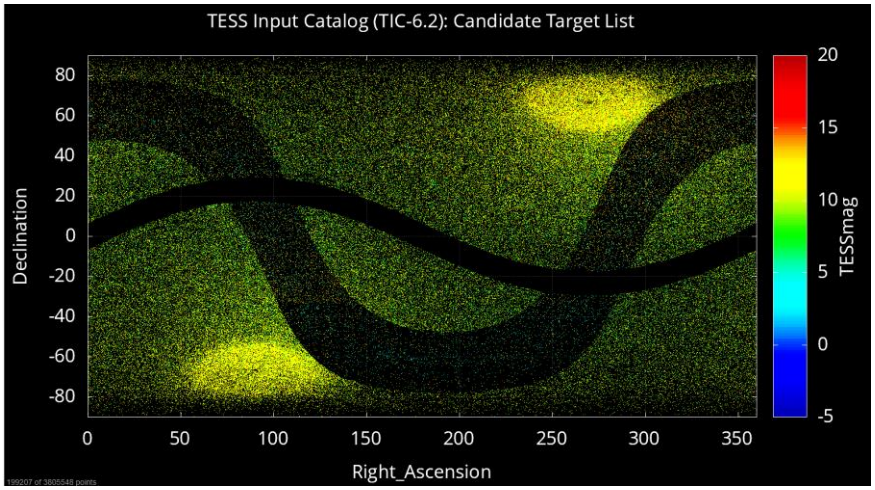

Figure 21: top 200,000 targets in CTL plotted in the magnitude in the TESS bandpass T; de-prioritization in the galactic and the ecliptic plane as well as a boosted prioritization at the ecliptic poles can be seen easily

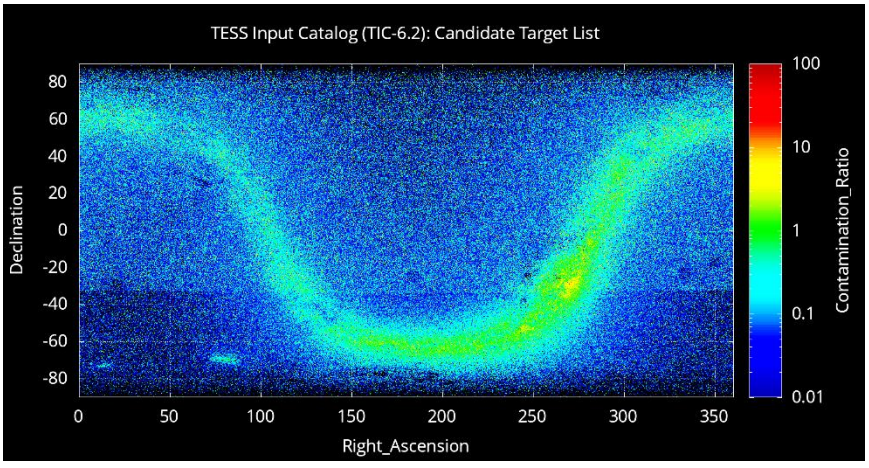

Figure 22: estimated logarithmic contamination ratio of the CTL catalog with significant contamination around the galactic plane; the prominent regions in the lower left are the Magellanic Clouds

[14] from filtergraph.com/tess_ctl/tic-6-ctl

5.6 Ground-based Analysis and Follow-Up

Mostly software from the Kepler mission will be used for TESS data reduction. The data reduction is similar to the methods presented in Chapter 4: pixel-level calibration, background subtraction, aperture photometry etc. Afterwards the selected transit light curves will be characterized and possible planets will be confirmed using ground-based imaging and spectroscopy. Moreover, planetary parameters like masses and radii will be figured out. Priority will be given to stars hosting planets with radii $< 4\ R_{\oplus}$. The planetary masses will be determined by Radial Velocity follow-up observations. All data will be made freely available through the MAST archive (Schlieder, 2017)

There are designated ground-based observatories for the follow-up surveys, nevertheless additional participation is welcomed by the TESS team. A follow-up campaign is also planned by an international team composed of the Landessternwarte Thüringen (TLS) in Tautenburg (Germany), the University of Graz with its Observatory at Lustbühel, and the Instituto des Astrofisica de Andalucia with its Observatorio de Sierra Nevada (Spain).

5.7 Anticipated Performance

The anticipated photometric performance for one hour of data is shown in Figure 23. The apparent magnitude I_C is plotted as a function of the standard deviation σ of the flux measurements. As one can see, the noise level for bright stars ($I_C < 8$) is set by the systematic noise created by random pointing variations. The CCD pixels have non-uniform quantum efficiencies, so a movement of a star on the CCD will cause changes in measured brightness. This effect is also called “spacecraft jitter”.

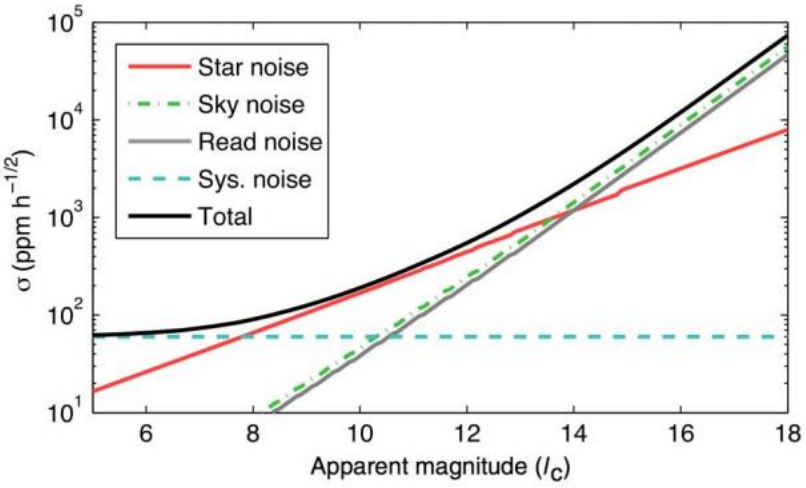

Figure 23: Anticipated photometric precision of TESS; photon counting noise of stars (red), noise from the zodiacal light (green), "spacecraft jitter" (blue) and the readout noise (grey) are shown (Ricker, et al., 2014)

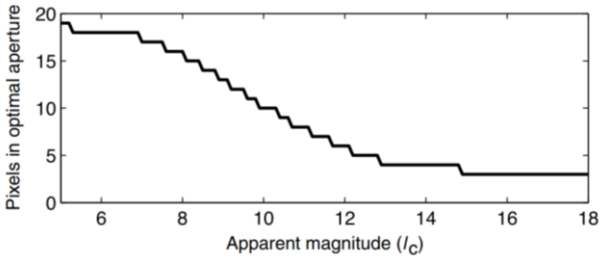

Figure 24: Number of pixels in the photometric aperture to optimize the signal-to-noise ratio *(Ricker, et al., 2014)*

In the range of $8 < I_C < 13$, photon counting noise dominates the error. The photometric precision for a star of 10^{th} apparent magnitude is about 200 ppm. This means TESS has a good precision for super Earths around bright stars. For the faintest stars ($I_C = 16$), the photometric precision drops to about 10^4 ppm (1 %), mainly due to the noise of the zodiacal light. (Ricker, et al., 2014)

The expected saturation limit of the CCDs central pixels is at $I_C = 7.5$. Nevertheless, a bright limit of $I_C = 4$ can be achieved using a photometric aperture covering so called "bleed trails". These trails are caused by saturated pixels which spread the excess charge over a column of pixels of the CCD (an effect also seen in the Kepler data). (Schlieder, 2017)

Barclay et al. (2018) use statistical models for the top 200,000 TESS targets, each hosting zero to a few planets, and the TESS noise model from above to predict the exoplanet occurrence rates:

* 2-min cadence data: 1,250 ± 70 exoplanets including 250 smaller than 2 $R_\oplus$
* 30-min cadence data:
  - 3,200 exoplanets orbiting bright dwarf stars
  - more than 10,000 exoplanets orbiting fainter stars

It is predicted that TESS will find about 500 planets around M-dwarfs. Most planets, however, will orbit stars larger than our sun. Using this simulation, Figure 25 was created with data from Sullivan et al. (2015) as a basis.

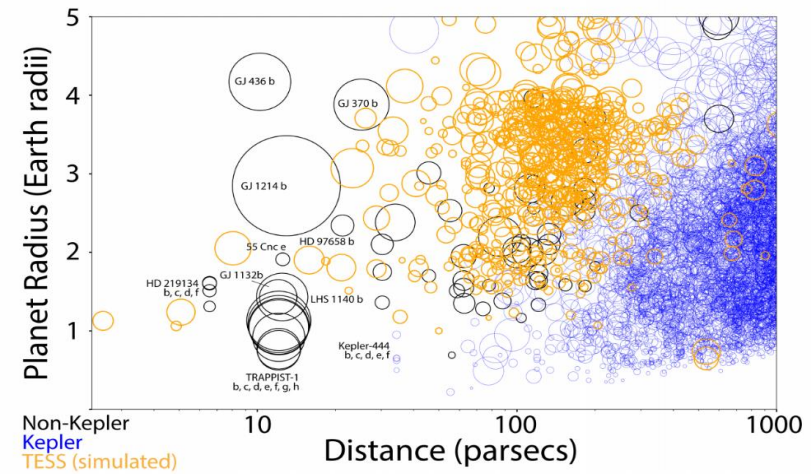

Figure 25: Diagram showing the planet radius as a function of the distance; size of the circle is proportional to the transit depth; Kepler planet candidates from Thompson et al. (2018) (blue), simulated 2-minute cadence detections (orange) and planets detected using other telescopes (black) (Barclay et al., 2018)

5.8 Current Status and Future Prospect

5.8.1 Commissioning and Current Status

After the launch in March, TESS underwent a commissioning phase lasting for about 60 days (see Figure 15). Commissioning was separated in 4 parts starting with about 7 days of spacecraft initialization. Operation checkouts for S-band receiver, star trackers, and propulsion system were done. In the following three days, TESS initialized the DHU and cameras saw first light and underwent initial tests. Afterwards, in phase 3, three fine pointing updates were performed and the first FFIs were taken. In phase 4, in which also the lunar encounter happened, target pixel masks as well as a guide star table were uploaded. A pixel response function was obtained by taking data from bright stars. (Schlieder, 2017)

At the moment of writing, TESS has already been searching for exoplanets since science operation officially began on July 25, 2018. The first data downlink is expected in August 2018.[15]

5.8.2 Prospect and Future TESS Missions

The 2-year main mission of the first all-sky space-based mission will provide the basis for many future satellites like JWST or PLATO. They will be able to investigate the most interesting of the thousands of new exoplanets TESS will discover as detailed as never before. Studying the atmospheres of exoplanets will be possible and will open our eyes to completely different or astonishing Earth-like worlds.

There are no initial obstacles for TESS not to continue observations after its 2-year primary mission. Bouma, et al. (2017) describe 6 possible scenarios for a TESS extended mission (visualized in Figure 26):

1. hemi: In the third year, observations of one hemisphere could be continued preferably with shifted longitudes to cover the "gaps" from the primary mission.

2. pole: One ecliptic pole could be focused for a longer period to extend the sensitivity of detecting planets with longer orbital periods.

3. hemi+ecl: observations like in the primary mission could be repeated, but with the observing sectors each shifted by 6° to the ecliptic. CVZ near the poles shrinks but the ecliptic can be covered.

4. ecl_long: Re-orientate the long axis of the FOV to the ecliptic. The ecliptic will be covered and follow-up investigations of K2 are possible. When ecliptic

[15] from https://www.nasa.gov/feature/goddard/2018/nasa-s-tess-spacecraft-starts-science-operations

observations are not possible due to scattered light from Earth and Moon, some field near the pole could be covered.

5. ecl_short: Similar to ecl_long but with the short axis of the FOV orientated along the ecliptic. This scenario covers more sky than ecl_long and has more overlap with the primary mission to enable follow-up observations.

6. allsky: Follow-up of almost all previously detected TESS targets by alternating between the hemispheres every 13.7 days covering the whole sky (observing sectors shifted in longitude by 6° as in hemi+ecl)

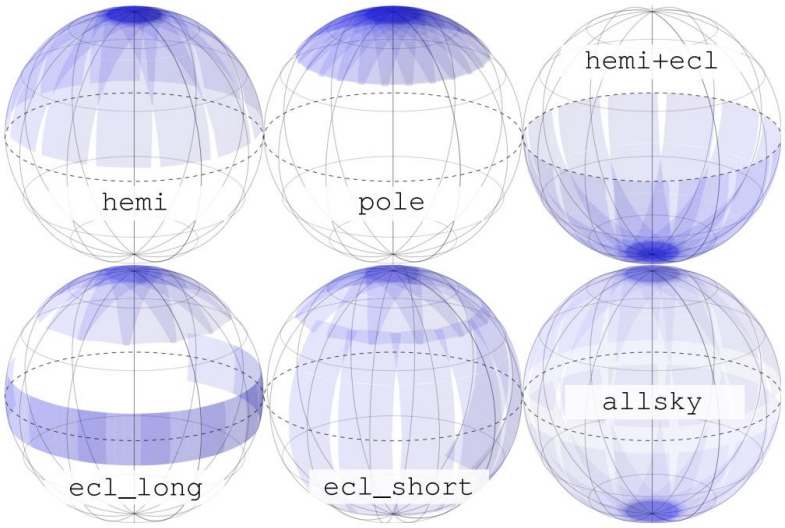

Figure 26: Possible observing sectors for a TESS extended mission after year 2 (Bouma, et al., 2017)

6. List of references

Andor Oxford Instruments, n.d. *Andor, CCD Sensor Architectures.* [Online]
Available at: http://www.andor.com/learning-academy/ccd-sensor-architectures-architectures-commonly-used-for-high-performance-cameras
[Accessed 06 08 2018].

Anon., 2018. *exoplanet.eu.* [Online]
Available at: http://exoplanet.eu/catalog/
[Accessed 05 08 2018].

Baader Planetarium, n.d. *Der Begriff sampling, over,- under- und good sampling.* [Online]
Available at: http://www.sbig.de/universitaet/glossar-htm/sampling.htm
[Accessed 06 08 2018].

Barclay, T., 2014. *K2 - Extending Kepler's Power to the Ecliptic.* [Online]
Available at: https://keplerscience.arc.nasa.gov/K2/ProposeTargets.shtml
[Accessed 06 08 2018].

Barclay, T., 2018. *TESS.* [Online]
Available at: https://heasarc.gsfc.nasa.gov/docs/tess/
[Accessed 06 08 2018].

Bathala, N. M., Rowe, J. F., Gilliland, R. L. & Jenknins, J. J., 2010. [Online]
Available at: https://arxiv.org/pdf/1001.0392.pdf
[Accessed 06 08 2018].

Bouma, L. G., Winn, J. N., Kosiarek, J. & McCullough, P., 2017. *arxiv.org.* [Online]
Available at: https://arxiv.org/pdf/1705.08891.pdf
[Accessed 06 08 2018].

Cameron, A. C., 2016. *Methods of Detecting Exoplanets.* s.l.:Springer.

Dichmann, D. J., Parker, J. J., Williams, T. W. & Mendelsohn, C. R., 2016. *NASA Goddard Flight Center.* [Online]
Available at:
https://ntrs.nasa.gov/archive/nasa/casi.ntrs.nasa.gov/20140007518.pdf
[Accessed 06 08 2018].

ESA, 2007. *ESA.* [Online]
Available at:
https://www.esa.int/spaceinimages/Images/2007/12/HD_189733b_and_surroundings
[Accessed 10 08 2018].

Garner, R., 2018. *NASA.* [Online]
Available at: https://www.nasa.gov/feature/goddard/2018/nasa-s-tess-spacecraft-

starts-science-operations
[Accessed 06 08 2018].

Gaudi, S. & Bennett, D., 2011. *Exploring Exoplanets with Microlensing.* [Online]
Available at: http://nexsci.caltech.edu/workshop/2011/
[Accessed 06 08 2018].

Gould, A. & Morgan, C. W., 2003. *iopscience.iop.org.* [Online]
Available at: http://iopscience.iop.org/article/10.1086/346131/pdf
[Accessed 06 08 2018].

Heiney, A., 2018. *NASA TESS Mission.* [Online]
Available at: https://blogs.nasa.gov/tess/
[Accessed 06 08 2018].

Jordi, C., Gebran, M. & Carrasco, J., 2010. *arxiv.org.* [Online]
Available at: https://arxiv.org/pdf/1008.0815.pdf
[Accessed 06 08 2018].

Kaltenegger, L., 2015. *Sind wir allein im Universum?: Meine Spurensuche im All.* s.l.:Ecowin.

Lissauer, J., 2018. *NASA Ames Research Center.* [Online]
Available at:
https://ntrs.nasa.gov/archive/nasa/casi.ntrs.nasa.gov/20180002120.pdf
[Accessed 06 08 2018].

MAST, 2008. *MAST Archive.* [Online]
Available at: http://archive.stsci.edu/
[Accessed 10 08 2018].

NASA, 2009. *NASA Kepler Mission Page.* [Online]
Available at: https://www.nasa.gov/mission_pages/kepler/multimedia/images/fov-kepler-drawing.html
[Accessed 06 08 2018].

NASA, 2009. *NASA National Aeronautics and Space Administration.* [Online]
Available at: https://www.jpl.nasa.gov/news/press_kits/Kepler-presskit-2-19-smfile.pdf
[Accessed 06 08 2018].

NASA, 2018. *5 Ways to Find a Planet.* [Online]
Available at: https://exoplanets.nasa.gov/5-ways-to-find-a-planet/
[Accessed 06 08 2018].

Perryman, M., 2011. *The Exoplanet Handbook.* Cambridge: Cambridge University Press.

Ricker, G. R. et al., 2014. *SPIE Digitsl Library.* [Online]
Available at: https://www.spiedigitallibrary.org/journals/Journal-of-Astronomical-Telescopes-Instruments-and-Systems/volume-1/issue-01/014003/Transiting-Exoplanet-Survey-Satellite/10.1117/1.JATIS.1.1.014003.full?SSO=1&tab=ArticleLink
[Accessed 06 08 2018].

Schlieder, J., 2017. *TESS Observatory Guide.* [Online]
Available at:
https://heasarc.gsfc.nasa.gov/docs/tess/docs/TESS_observatory_guide_v1.1.pdf
[Accessed 06 08 2018].

SDSS, n.d. *Sloan Digital Sky Survey / SkyServer.* [Online]
Available at: http://skyserver.sdss.org/dr4/en/proj/advanced/hr/radius1.asp
[Accessed 06 08 2018].

Spaceflight 101, 2018. *Spaceflight 101.* [Online]
Available at: http://spaceflight101.com/tess/
[Accessed 06 08 2018].

Stassun, K. G. et al., 2018. *arxiv.org.* [Online]
Available at: https://arxiv.org/pdf/1706.00495.pdf
[Accessed 06 08 2018].

Sullivan, P. W. et al., 2017. *arxiv.org.* [Online]
Available at: https://arxiv.org/pdf/1506.03845.pdf
[Accessed 06 08 2018].

Wilson, P. A., 2017. *The exoplanet transit method.* [Online]
Available at: https://www.paulanthonywilson.com/exoplanets/exoplanet-detection-techniques/the-exoplanet-transit-method/
[Accessed 06 08 2018].

Wright, J. T. & Gaudi, S. B., 2012. *Exoplanet Detection Methods.* [Online]
Available at: https://arxiv.org/pdf/1210.2471.pdf
[Accessed 06 08 2018].

7. Appendix

Example for a polynomial relations to calculate the TESS magnitude T:

The relations between T and the Gaia photometry valid for $\log g \geq 3$ is given by

$$T(\pm 0.010) = G + 0.00942(G - K_S)^3 + 0.0028(G - K_S)^2 - 0.35664(G - K_S) + 0.0125$$

$$valid\ for - 0.3 \leq G - K_S \leq 2.5$$

and

$$T(\pm 0.019) = G + 0.02925(G - K_S)^3 - 0.29659(G - K_S)^2 + 0.60877(G - K_S) - 0.8676$$

$$valid\ for\ 2.5 \leq G - K_S \leq 5.2$$

The G and the K_S represent magnitudes in different filters (passbands) in the photometric system of the Gaia mission (see Jordi, et al., 2010). Similar polynomial relations are found for the magnitudes in other filters like the J or H passband. These filters are designed for the near-infrared region of the electromagnetic spectrum. As two magnitudes are necessary to evaluate these equations, the TESS magnitude for faint stars, for which only one magnitude is available, is estimated by an offset. (Stassun, et al., 2018)

Determination of T_{eff}:

As an example, the relations for non-giants in the ranges V – KS: [−0.10, 5.05] and [Fe/H]: [−0.9, +0.4] are presented here.

$$X = V - K_S(de - reddened)$$

$$Y = [\mathrm{Fe/H}]$$

$$\theta = 0.54042 + 0.23676X - 0.00796X^2 - 0.03798XY - 0.05413Y - 0.00448Y^2$$

$$T_{eff}[\mathrm{K}] = \frac{5040}{\theta}$$

The uncertainty of this T_{eff} value due to the calibration is 2% and in general the photometric error also has to be taken into account. (Stassun, et al., 2018)